ELSEVIER

Contents lists available at ScienceDirect

# Separation and Purification Technology

journal homepage: www.elsevier.com/locate/seppur



# Raman imaging of membrane fouling

Samar Azizighannad<sup>a</sup>, Worawit Intrchom<sup>b</sup>, Somenath Mitra<sup>b,\*</sup>

- <sup>a</sup> Department of Materials Science and Engineering, New Jersey Institute of Technology, Newark, NJ 07102, USA
- <sup>b</sup> Department of Chemistry and Environmental Sciences, New Jersey Institute of Technology, Newark, NJ 07102, USA



ARTICLE INFO

Keywords:
Membrane
Desalination
Membrane distillation
Raman imaging
Water treatment

### ABSTRACT

Membrane processes are widely used in industrial applications such water purification, food processing and pharmaceutical manufacturing. During their operation, the accumulation of foulants in membrane pores and on membrane surfaces lead to the reduction in flux, membrane lifetime and increase in operational cost, and the understanding of the fouling phenomenon is important for mitigating these problems. In this paper we report the application of Raman chemical imaging as a means of identify and map foulants on a membrane surface. The surface of a Polytetrafluoroethylene (PTFE) membrane was studied by Raman chemical imaging before and after fouling during desalination via membrane distillation. Information about location and concentration of three different salts namely CaSO<sub>4</sub>, BaSO<sub>4</sub> and CaCO<sub>3</sub> was studied. The three salts showed different distribution patterns, and their distribution was analyzed by correlation mapping and multivariate curve resolution. It was observed that CaSO<sub>4</sub> agglomerated in specific places while the BaSO<sub>4</sub> and CaCO<sub>3</sub> were more distributed. Raman imaging appears to be a powerful tool for studying membrane foulants and can be effective in identifying the distribution of different species on a membrane surface.

# 1. Introduction

Membrane based separation processes are widely used in diverse applications such as wastewater treatment [1-3], water purification [4,5], food and beverage processing [6-8] and pharmaceutical applications [9-11]. They offer advantages such as high selectivity, low energy and chemical requirements, and small equipment footprint [12]. A major challenge in membrane separations is fouling that impairs their operation and lower efficiency [12-16]. Fouling is a common phenomenon in pressure-driven membrane processes such as reverse osmosis (RO), nanofiltration (NF), ultrafiltration (UF) and microfiltration (MF) [17]. However, this phenomenon is also prevalent in non-pressure driven processes especially when salt water is involved, for example, forward osmosis (FO) and membrane distillation (MD) [18,19]. There are four major types of foulants, namely particulates and colloids, organic foulants, inorganic scalants and biofouling. The presence of these foulants in membrane pores or/and on membrane surface directly leads to the reduction of flux and membrane lifetime and also increase operational and maintenance cost [12]. Therefore, to clearly understand and mitigate membrane fouling, the monitoring of fouling is necessary.

Membrane fouling is often monitored via operation parameters such as the permeate flux profiles, the changes in pressure and the characteristics of the permeate [14]. Instruments such as ultrasonic time-

domain reflectometry (UTDR) and electrical impedance spectroscopy (EIS) have been used to investigate the membrane fouling as in-situ methods [20-22]. While they are real-time approaches, they do not provide in-depth details of foulant formation on the membrane surface. To study the deposition of the foulants on a membrane in detail [14], variety of instruments such as energy dispersive X-ray (EDX) Spectroscopy, X-ray photo spectroscopy (XPS), X-ray diffractometry (XRD) [14], scanning electron microwave (SEM) [23], atomic force microscopy (AFM), and confocal scanning laser microscopy (CSLM) have been used to study foulants [14,24]. Extended Derjaguin-Landau-Verwey-Overbeek (XDLVO) and density functional theory (DFT) have been used to study the role of surface morphology on alginate adhesive fouling [15]. Both composition and formation of foulants on the membrane are important and complimentary information that are needed to develop deeper understanding of fouling. Recently, the Fourier transform infrared (ATR-FTIR) has been applied to analyze the composition and the image of the fouled membrane from pig manure separation [25].

Dispersive Raman spectroscopy is evolving to be powerful tool for the identification and imaging of a wide range of compounds [26–28] such as pharmaceutical products, polymers, papers and glass [26]. Some of the advantages include minimal sample preparation, analysis in the far IR, and with a 1-µm excitation laser spot size it is an excellent

E-mail address: Somenath.mitra@njit.edu (S. Mitra).

<sup>\*</sup> Corresponding author.

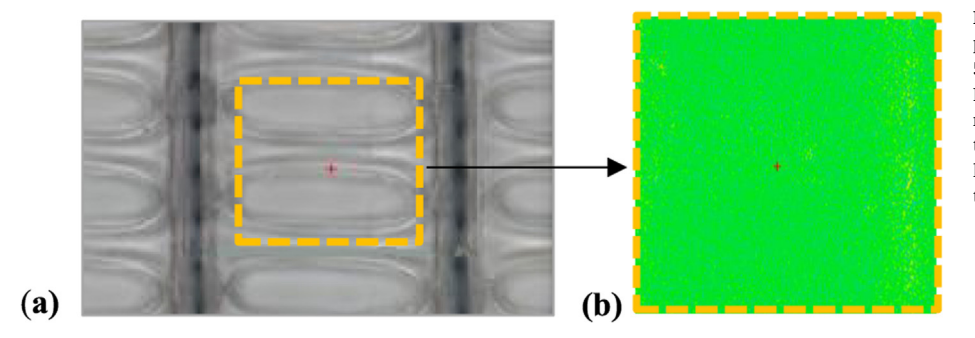
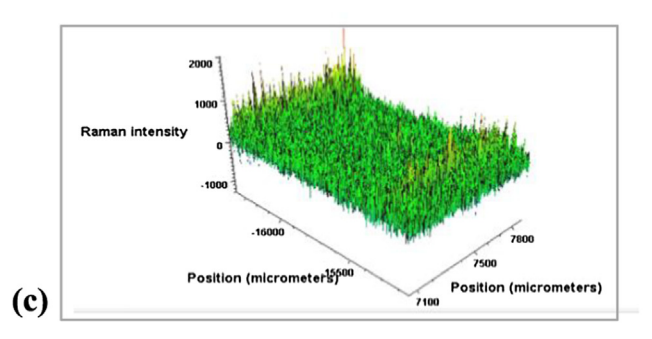
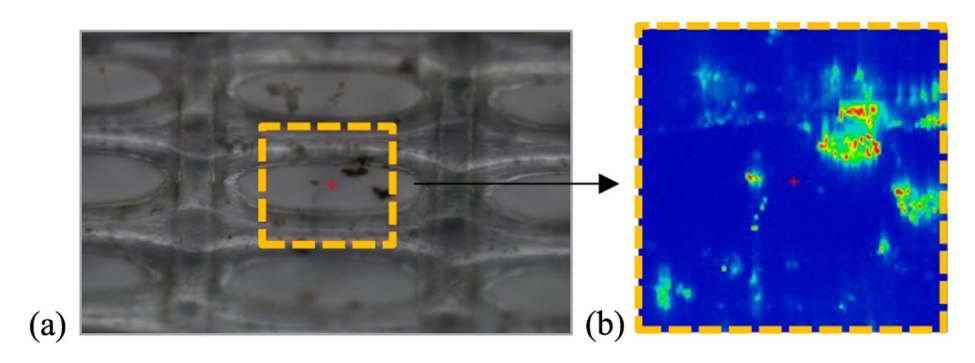
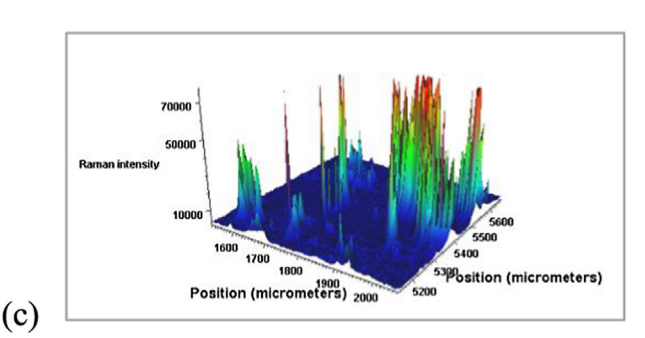


Fig. 1. (a)  $10 \times$  magnification optical image of the plain PTFE membrane, (b) Correlation mapping of  $50 \times 50$ -µm area (yellow dotted area) of the plain PTFE membrane, (c) 3D plotted correlated chemical image of the plain PTFE membrane. (For interpretation of the references to color in this figure legend, the reader is referred to the web version of this article.)





**Fig. 2.** (a)  $10 \times$  magnification optical image of the fouled PTFE membrane, (b) Correlation mapping of  $50 \times 50$ -μm area (yellow dotted area) of the fouled PTFE membrane: Red color indicates the highest concentration of foulant, and blue color indicates areas without foulant, (c) 3D plotted correlated chemical image of the fouled PTFE membrane showing distribution of the salts. (For interpretation of the references to color in this figure legend, the reader is referred to the web version of this article.)



technique when high spatial resolution is needed [29]. It is a facile, nondestructive method that integrates chemical imaging to can provide information about composition and distribution of the sample components. Variety of methods has been used to analyze images that has been collected by Raman [30]. Correlation mapping and Multivariate Cure Resolution (MCR) are two well-known approaches that have been used to analyze Raman image.

Correlation mapping based upon known reference spectrum or a spectrum from the acquired data [31] shows spectral changes associated with a sample, and is represented in a 2-dimensional plot that differentiates the regions of varying Raman intensity (or concentration). It can also be plotted in 3-dimensional (3D) to show the surface distribution to provide a better visualization of the selected area [32].

Unlike correlation mapping which scales intensity based on acquired spectrum, Multivariate Curve Resolution (MCR) is a statistical method that does not require reference spectra. The main difference between correlation mapping and MCR is that correlation mapping uses one reference spectra and applies that to the image, but MCR uses several spectral components and combines the experimental data [33]. MCR can be used to extract critical information about composition of the chemicals [30,34] and map a surface based upon composition, which is often presented via color coding. Correlation mapping can also extract composition based on a single spectrum, but it could only be done one component at a time. Other reported advantages of Raman imaging are high sensitivity, resolved peaks that enable univariate data analysis and reduce data complexity, and good quantitation [26,28,29,35,36]. For

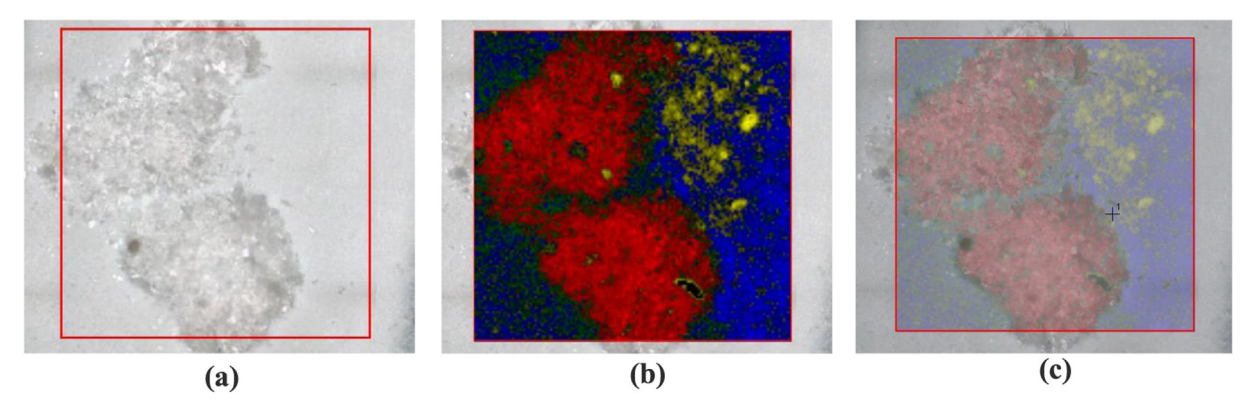


Fig. 3. a) 5 × 5-μm area optical image with 50 × magnification of fouled PTFE membrane and salts, b) MCR image of the membrane and salts (Blue: Membrane, Red: CaSO<sub>4</sub>, Green: BaSO<sub>4</sub>, Yellow: CaCO<sub>3</sub>), c) Combination of optical and MCR image. (For interpretation of the references to color in this figure legend, the reader is referred to the web version of this article.)

example, Raman imaging for Graphene sheets has been carried out based on the G-band [37] and Raman Imaging for plants have provided information about structure, composition and properties of the plant cells [38]. Raman Chemical Imaging has been applied to biological, biomedical and pharmaceutical studies. It has been used to study morphology and identify the tissues and abnormal changes resulting from diseases have been detected [26]. It is has also been applied to clinical diagnosis to identify microorganisms in cellular samples [28,35], however being a macro-scale technique, it has certain limitations for biological samples [26]. In general, while there are several reports related to Raman Imaging of different kinds of samples, this technique is yet to be applied in membrane science especially for monitoring fouling. The objective of this research is the detection and imaging of the distribution of inorganic salts deposited on a fouled membrane via Raman Imaging to demonstrate the applicability of this technique in the study of membrane fouling.

## 2. Experimental

Thermo Scientific DXRxi Raman imaging microscope was used in this study and a 532 nm laser was used on the 50  $\times$  50 to 5  $\times$  5- $\mu m$ areas of the sample. Exposure time was 0.05 s for 5 scans. Optical images of the membranes with 10× and 50× magnification followed by analyzing image with OMNICxi imaging software. Raman chemical image was acquired and processed by OMNICxi software. This software can be used to apply different profiles to the image based on needs. It can differentiate components based on the Raman spectra library. The software collects Raman spectrum of the sample and based on the selected profile it can generate information about the components and their distribution in the sample. Correlation and MCR profiles were used to generate detailed information and map the surface based on chemical composition. Furthermore, the Raman spectrum of each mapped area has been used to identify each component. 3D plot based on Raman intensity also provided better understanding of how components are distributed on the sample surface.

# 3. Sample preparation

In this study, a polytetrafluoroethylene (PTFE) membrane with an effective contact area of  $11.94~\rm cm^2$  was used for desalination via direct contact membrane distillation (DCMD) during which salts were deposited on it. The feed solution undergoing MD was prepared by dissolving  $2.5~\rm g$  of  $CaSO_4$ ,  $BaSO_4$ , and  $CaCO_3$  in  $1000~\rm mL$  of deionized water. The hot feed at temperature of  $70~\rm ^{\circ}C$  and pH of  $7.4-7.5~\rm ^{\circ}C$  was circulated through the feed side of the membrane by peristaltic pumps (MasterFlex Easy Load, Cole-Parmer, USA) at a flow rate of  $150~\rm mL/$  minute while the countercurrent flow of cold distilled water was passed

on the permeate side at a flow rate of 200 mL/min. After 6 h of MD, the membrane was taken out and dried in the vacuum oven at 60 °C until its weight was constant. Raman Chemical Imaging of the plain PTFE membrane and PTFE membrane fouled with salts namely  $CaSO_4$ ,  $BaSO_4$  and  $CaCO_3$  was carried out.

#### 4. Results and discussion

The Raman Microscope provided high resolution optical images which was complemented by the detailed chemical image generated by Raman spectroscopy. Correlation mapping and MCR analysis was combined to map the components in this sample. Multivariate curve resolution (MCR) that can extract components from chemical maps and facilitate component identification, even in cases where there is no prior knowledge about the chemical components in the sample. In this study, the spatial distribution of three different salts on top of the membrane which leads to membrane fouling was studied. Raman microscopy helped analyze selected sample area with a high spatial resolution.

Fig. 1a shows the  $10\times$  magnification optical image of plain PTFE membrane before desalination via MD, or without any foulant. As expected, no residual substance was seen on the membrane surface. Correlation mapping was applied to the  $50\times50$ -µm area (yellow dotted area) of optical image in Fig. 1b. Since there was a consistent Raman intensity all over the membrane, correlation map presented a uniform chemical image. Correlation chemical mapping (Fig. 1b) corresponded to the relative intensity of the peak across the sample. Fig. 1c is the 3D plot of correlated chemical mapping of the PTFE membrane which showed uniform distribution of the membrane material.

In the next step, Raman mapping of the fouled membrane was carried out. To study the distribution of the salts, first it was important to survey the membrane surface. Fig. 2a presents the  $10\times$  magnification optical image of the fouled membrane. To study the fouling pattern, a  $50\times50$ -µm area of the fouled section was selected. Fig. 2b shows the correlation mapping of the membrane fouled with CaSO<sub>4</sub>, BaSO<sub>4</sub>, CaCO<sub>3</sub>. Correlation map showed the distribution of salt on the membrane surface, where the red color represented the areas with highest concentrations. Fig. 2C is a 3D plot that shows the distribution of salts on the membrane surface. The 3D plot also provided a simple representation of the salt distribution and regions of high fouling.

Furthermore, to study the details on the fouled membrane a smaller area of 5  $\times$  5- $\mu m$  was selected by 50  $\times$  magnification in order to study the surface composition. It was not possible to differentiate the salts in the correlation image, so MCR profile including 3 salts and membrane itself was applied to the spectra. Fig. 3a shows the optical image of 5  $\times$  5- $\mu m$  area followed by running MCR profile presented in Fig. 3b. The identification and distribution of each slat is shown in Fig. 3b (Blue:

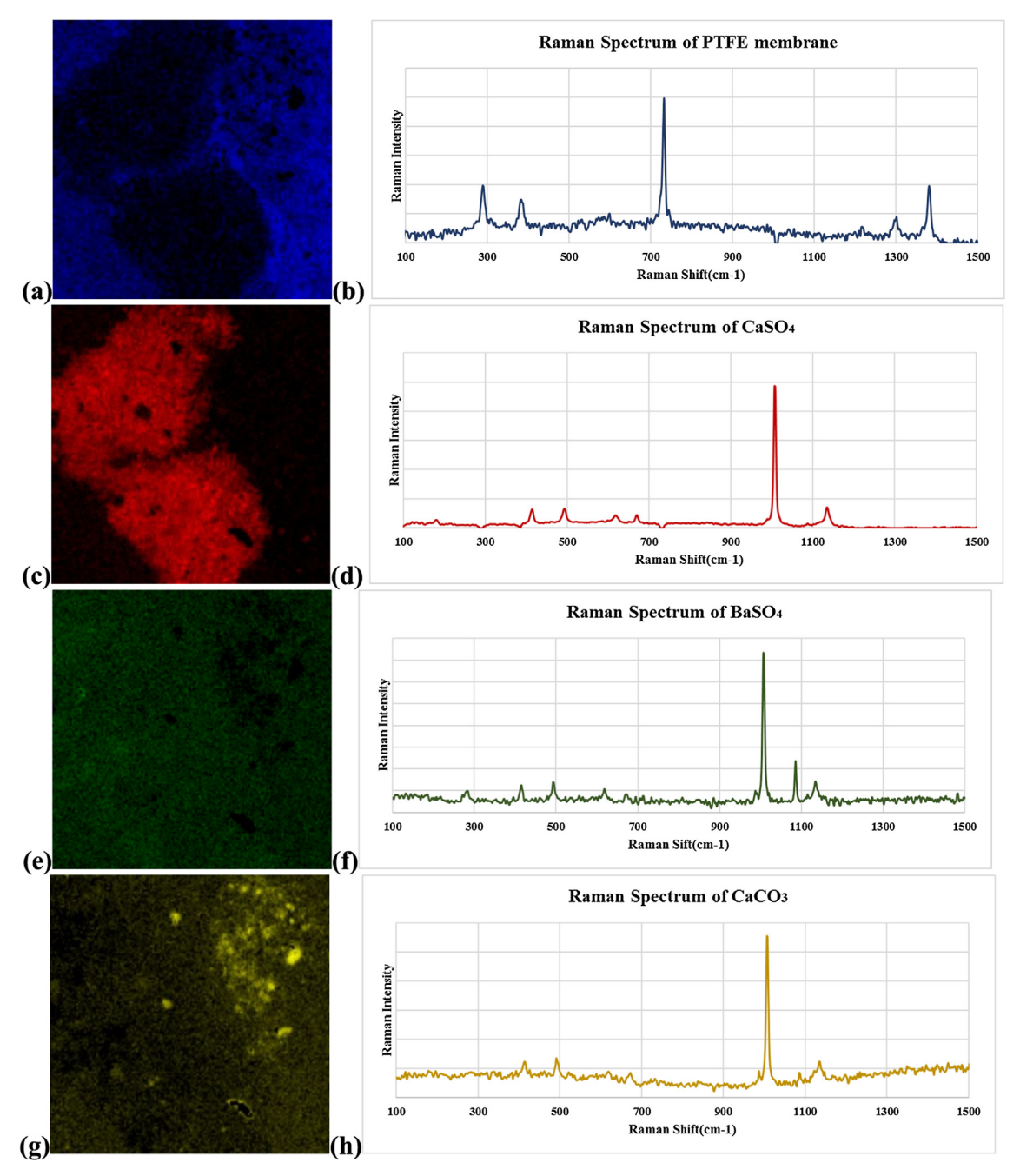


Fig. 4. Composition of fouled PTF membrane: (Blue: Membrane, Red:  $CaSO_4$ , Green:  $BaSO_4$ , Yellow:  $CaCO_3$ ); (a) MCR profile of  $5 \times 5$ - $\mu$ m area of the fouled PTFE membrane, (b) Raman Spectrum of the fouled PTFE membrane, (c) MCR image of the area including  $CaSO_4$ , (d) Raman Spectrum of  $CaSO_4$ , (e) MCR image of the area including  $CaCO_3$ , (f) Raman Spectrum of  $CaCO_3$ . (For interpretation of the references to color in this figure legend, the reader is referred to the web version of this article.)

Membrane, Red: CaSO<sub>4</sub>, Green: BaSO<sub>4</sub>, Yellow: CaCO<sub>3</sub>). The combination of the MCR image and optical image is presented in Fig. 3c can be used to analyze location and distribution of each component. In order to identify each salt, Raman spectra for each component represented by a different color is presented in Fig. 4a to h. Each of Fig. 4a to h display one component and the corresponding Raman spectrum. PTFE (Fig. 4a and b) was identified from OMNICxi library. The areas that was all covered with salts (black portion of Fig. 4a) showed no Raman intensity corresponding to PTFE. Fig. 4c, d is related to distribution of CaSO<sub>4</sub> on the fouled membrane based on the corresponding Raman spectrum of that specie. It is seen that the CaSO<sub>4</sub> was deposited as a large agglomerate. Fig. 4e and f are related to BaSO<sub>4</sub> distribution based on its corresponding spectrum. Compared to CaSO<sub>4</sub>, BaSO<sub>4</sub> showed a more

uniform dispersion over the membrane. Lastly,  $CaCO_3$  distribution and its spectrum are presented in Fig. 4g and h.  $CaCO_3$  was also found to be distributed in most areas of the membrane. Solubility product (Ksp) of  $CaSO_4$  was higher than  $CaCO_3$  and  $BaSO_4$ . Therefore,  $CaCO_3$  and  $BaSO_4$  tended to precipitate faster than  $CaSO_4$  and they precipitated over a larger area which is evident from the images [39]. This is in line with what has been reported before related to the aggregation kinetics of  $CaSO_4$ . Growth of  $CaSO_4$  is known to happen in all the directions. Also, the particle size was larger than the other two salts and was as high as 5 µm [40]. Detection limit corresponds to the lowest concentration of the samples that can be detected by Raman Imaging. It was measured using a method published before [41]. The detection limit was found to be 0.01 mg/ml for  $CaSO_4$  and for  $BaSO_4$  and 0.03 mg/ml for  $CaCO_3$ .

In general, Raman chemical imaging has several advantages over conventional techniques such as confocal scanning laser microscopy (CSLM) and scanning electron microscopy (SEM). Optical techniques such as CSLM provides image but is not able to distinguish between different foulants and their distribution. SEM has been used to use fouling distribution in membranes and can provide very useful information. Chemical information in SEM can be limited, although energy dispersive X-Ray spectroscopy (EDS) mapping can provide some useful elemental information. However, that may not provide enough distinction between different chemical species, for example in this case, EDS could not be used to distinguish between CaCO<sub>3</sub> and CaSO<sub>4</sub>. Moreover, SEM is an expensive and complex analytical system where is Raman imaging is a relatively simple technique and can be implied insitu on membrane surfaces. Compact hand-held Raman spectrometers are commercially available and can be used in the field [42].

### 5. Conclusions

This study presents the application of Raman chemical imaging to identify and differentiate inorganic salts on a fouled membrane surface. PTFE Membrane fouled during desalination by membrane distillation was studied and the distribution of CaSO<sub>4</sub>, BaSO<sub>4</sub> and CaCO<sub>3</sub> on the membrane surface was mapped by Raman imaging. The location of each salt could be successfully identified based on the Raman Spectra. It was observed that CaSO<sub>4</sub> tended to agglomerate and settle on the certain areas while BaSO<sub>4</sub> and CaCO<sub>3</sub> were distributed over the whole membrane. Information such as this can be used to study the mechanism of fouling. It is concluded that Raman chemical imaging is an effective approach to survey membrane surfaces as well as fouling. In general, it is a novel, fast and non-destructive method that can be used to survey membrane surface and can be valuable in understanding surface coverage from different foulants which is the major challenge in membrane processes.

# **Declaration of Competing Interest**

The authors declare that they have no known competing financial interests or personal relationships that could have appeared to influence the work reported in this paper.

## Acknowledgements

This work was funded by a grant from the (National Science Foundation) NSF and Membrane Science, Engineering and Technology Center) MAST Center. Any opinions, findings, and conclusions or recommendations expressed in this material are those of the author(s) and do not necessarily reflect the views of the NSF and MAST Center. Funding from the Ida C. Fritts Chair at New Jersey Institute of Technology (NJIT) is also acknowledged. The Otto York Center for Environmental Engineering and Science is acknowledged for the use of their instruments.

## References

- [1] H. Ozgun, R.K. Dereli, M.E. Ersahin, C. Kinaci, H. Spanjers, J.B. van Lier, A review of anaerobic membrane bioreactors for municipal wastewater treatment: integration options, limitations and expectations, Sep. Purif. Technol. 118 (2013) 89–104.
- [2] J. Lee, H.-R. Chae, Y.J. Won, K. Lee, C.-H. Lee, H.H. Lee, I.-C. Kim, J.-M. Lee, Graphene oxide nanoplatelets composite membrane with hydrophilic and antifouling properties for wastewater treatment. J. Membr. Sci. 448 (2013) 223–230.
- [3] H.A. Qdais, H. Moussa, Removal of heavy metals from wastewater by membrane processes: a comparative study, Desalination 164 (2004) 105–110.
- [4] Y. Han, Z. Xu, C. Gao, Ultrathin graphene nanofiltration membrane for water purification, Adv. Funct. Mater. 23 (2013) 3693–3700.
- [5] A.G. Fane, R. Wang, M.X. Hu, Synthetic membranes for water purification: status and future, Angew. Chem. Int. Ed. 54 (2015) 3368–3386.
- [6] A.W. Mohammad, C.Y. Ng, Y.P. Lim, G.H. Ng, Ultrafiltration in food processing industry: review on application, membrane fouling, and fouling control, Food Bioprocess Technol. 5 (2012) 1143–1156.

- [7] Z. Cui, H. Muralidhara, Membrane Technology: A Practical Guide to Membrane Technology and Applications in Food and Bioprocessing, Elsevier, 2010.
- [8] A.Y. Tamime, Membrane Processing: Dairy and Beverage Applications, John Wiley & Sons, 2012
- [9] L. Peeva, J. da Silva Burgal, I. Valtcheva, A.G. Livingston, Continuous purification of active pharmaceutical ingredients using multistage organic solvent nanofiltration membrane cascade, Chem. Eng. Sci. 116 (2014) 183–194.
- [10] K. Gethard, O. Sae-Khow, S. Mitra, Carbon nanotube enhanced membrane distillation for simultaneous generation of pure water and concentrating pharmaceutical waste, Sep. Purif. Technol. 90 (2012) 239–245.
- [11] R. Abejón, A. Garea, A. Irabien, Analysis and optimization of continuous organic solvent nanofiltration by membrane cascade for pharmaceutical separation, AIChE J. 60 (2014) 931–948.
- [12] W. Guo, H.-H. Ngo, J. Li, A mini-review on membrane fouling, Bioresour. Technol. 122 (2012) 27–34.
- [13] S. Lee, C. Boo, M. Elimelech, S. Hong, Comparison of fouling behavior in forward osmosis FO) and reverse osmosis (RO), J. Membr. Sci. 365 (2010) 34–39.
- [14] P. Goh, W. Lau, M. Othman, A. Ismail, Membrane fouling in desalination and its mitigation strategies, Desalination 425 (2018) 130–155.
- [15] R. Li, Y. Lou, Y. Xu, G. Ma, B.-Q. Liao, L. Shen, H. Lin, Effects of surface morphology on alginate adhesion: molecular insights into membrane fouling based on XDLVO and DFT analysis, Chemosphere 233 (2019) 373–380.
- [16] Y. Chen, G. Yu, Y. Long, J. Teng, X. You, B.-Q. Liao, H. Lin, Application of radial basis function artificial neural network to quantify interfacial energies related to membrane fouling in a membrane bioreactor, Bioresour. Technol. 293 (2019) 122103
- [17] S. Shirazi, C.-J. Lin, D. Chen, Inorganic fouling of pressure-driven membrane processes—a critical review, Desalination 250 (2010) 236–248.
- [18] Y. Chun, D. Mulcahy, L. Zou, I. Kim, A short review of membrane fouling in forward osmosis processes, Membranes 7 (2017) 30.
- [19] L.D. Tijing, Y.C. Woo, J.-S. Choi, S. Lee, S.-H. Kim, H.K. Shon, Fouling and its control in membrane distillation—a review, J. Membr. Sci. 475 (2015) 215–244.
- [20] X. Li, J. Li, J. Wang, H. Zhang, Y. Pan, In situ investigation of fouling behavior in submerged hollow fiber membrane module under sub-critical flux operation via ultrasonic time domain reflectometry, J. Membr. Sci. 411 (2012) 137–145.
- [21] X. Li, J. Li, J. Wang, H. Wang, C. Cui, B. He, H. Zhang, Direct monitoring of sub-critical flux fouling in a horizontal double-end submerged hollow fiber membrane module using ultrasonic time domain reflectometry, J. Membr. Sci. 451 (2014) 226–233.
- [22] L. Sim, Z. Wang, J. Gu, H. Coster, A. Fane, Detection of reverse osmosis membrane fouling with silica, bovine serum albumin and their mixture using in-situ electrical impedance spectroscopy, J. Membr. Sci. 443 (2013) 45–53.
- [23] W. Yu, Y. Liu, Y. Xu, R. Li, J. Chen, B.-Q. Liao, L. Shen, H. Lin, A conductive PVDF-Ni membrane with superior rejection, permeance and antifouling ability via electric assisted in-situ aeration for dye separation, J. Membr. Sci. 581 (2019) 401–412.
- [24] M. Ferrando, A. Ro'žek, M. Zator, F. Lopez, C. Güell, An approach to membrane fouling characterization by confocal scanning laser microscopy, J. Membr. Sci. 250 (2005) 283–293
- [25] O. Thygesen, M.A. Hedegaard, A. Zarebska, C. Beleites, C. Krafft, Membrane fouling from ammonia recovery analyzed by ATR-FTIR imaging, Vib. Spectrosc. 72 (2014) 119–123.
- [26] S. Lohumi, M.S. Kim, J. Qin, B.-K. Cho, Raman imaging from microscopy to macroscopy: quality and safety control of biological materials, TrAC, Trends Anal. Chem. 93 (2017) 183–198.
- [27] S. Sahu, D.L. Exline, M.P. Nelson, Identification of thaumasite in concrete by Raman chemical imaging, Cem. Concr. Compos. 24 (2002) 347–350.
- [28] M.F. Escoriza, J.M. VanBriesen, S. Stewart, J. Maier, P.J. Treado, Raman spectroscopy and chemical imaging for quantification of filtered waterborne bacteria, J. Microbiol. Methods 66 (2006) 63–72.
- [29] A. Wang, R.L. Korotev, B.L. Jolliff, Z. Ling, Raman imaging of extraterrestrial materials, Planet. Space Sci. 112 (2015) 23–34.
- [30] L. Zhang, M.J. Henson, S.S. Sekulic, Multivariate data analysis for Raman imaging of a model pharmaceutical tablet, Anal. Chim. Acta 545 (2005) 262–278.
- [31] R.M.J. Mark, H. Wall, Elena Polyakova, Uncovering the Secrets Governing the Chemical Vapor Deposition of Graphene with Rapid Raman Imaging in, Thermo Scientific.
- [32] Y.H. El-Sharkawyi, Detection and characterization of human teeth caries using 2D correlation Raman spectroscopy, J. Biomed. Phys. Eng. 9 (2019) 167–178.
- [33] J.P. Smith, F.C. Smith, K.S. Booksh, Multivariate curve resolution-alternating least squares (MCR-ALS) with Raman imaging applied to lunar meteorites, Appl. Spectrosc. 72 (2017) 404–419.
- [34] G.P.S. Smith, C.M. McGoverin, S.J. Fraser, K.C. Gordon, Raman imaging of drug delivery systems, Adv. Drug Deliv. Rev. 89 (2015) 21–41.
- [35] B. Durrant, M. Trappett, D. Shipp, I. Notingher, Recent developments in spontaneous Raman imaging of living biological cells, Curr. Opin. Chem. Biol. 51 (2019) 138–145.
- [36] Y. Shen, F. Hu, W. Min, Raman imaging of small biomolecules, Annu. Rev. Biophys. 48 (2019) 347–369.
- [37] D. Graf, F. Molitor, K. Ensslin, C. Stampfer, A. Jungen, C. Hierold, L. Wirtz, Raman imaging of graphene, Solid State Commun. 143 (2007) 44–46.
- [38] N. Gierlinger, M. Schwanninger, The potential of Raman microscopy and Raman imaging in plant research, Spectroscopy 21 (2007) 69–89.
- [39] A. Neira-Carrillo, P. Mercadé-Jaque, M. Diaz-Dosque, C. Tapia-Villanueva, M. Yazdani-Pedram, Influence of chitosan grafted poly(vinyl sulfonic acid) as template on the calcium carbonate crystallization, J. Iran. Chem. Soc. 8 (2011) 811–824.

- [40] F. Sariman, A.P. Bayuseno, S. Muryanto, Crystallization of barium sulfate (BaSO4) in a flowing system: influence of malic acid on induction time and crystal phase transformation, in: MATEC Web of Conferences, 2018.
- [41] G. Massonnet, P. Buzzini, F. Monard, G. Jochem, L. Fido, S. Bell, M. Stauber, T. Coyle, C. Roux, J. Hemmings, H. Leijenhorst, Z. Van Zanten, K. Wiggins, C. Smith, S. Chabli, T. Sauneuf, A. Rosengarten, C. Meile, S. Ketterer, A. Blumer,
- Raman spectroscopy and microspectrophotometry of reactive dyes on cotton fibres: analysis and detection limits, Forensic Sci. Int. 222 (2012) 200–207.

  [42] A. Lanzarotta, M.M. Kimani, M.D. Thatcher, J. Lynch, M. Fulcher, M.R. Witkowski,
- [42] A. Lanzarotta, M.M. Kimani, M.D. Thatcher, J. Lynch, M. Fulcher, M.R. Witkowski, J.S. Batson, Evaluation of suspected counterfeit pharmaceutical tablets declared to contain controlled substances using handheld Raman spectrometers, J. Forensic Sci., n/a.